Journal of Applied Polymer Science

# Morphology, Structure, and Properties of Poly(lactic acid) Microporous Films Containing Poly(butylene terephthalate) Fine Fibers Fabricated by Biaxial Stretching

**Chavakorn Samthong,[1] Jiraporn Seemork,[2] Shogo Nobukawa,[2] Masayuki Yamaguchi,[2] Piyasan Praserthdam,[1] Anongnat Somwangthanaroj[1]**

[1]Department of Chemical Engineering, Faculty of Engineering, Chulalongkorn University, Bangkok 10330, Thailand
[2]School of Materials Science, Japan Advanced Institute of Science and Technology, 1-1 Asahidai, Nomi, Ishikawa 923-1292, Japan
Correspondence to: A. Somwangthanaroj (E-mail: anongnat.s@chula.ac.th)

**ABSTRACT:** The effects of size and shape, i.e., sphere and fiber, of dispersed poly(butylene terephthalate) (PBT) in poly(lactic acid) (PLA) matrix on the morphology and porous structure of the biaxially stretched films are comparatively investigated. Scanning electron microscope results confirm that the PBT fine fibers can be produced by melt-stretching following by fast quenching. Rheological characterization reveals the random network structure of PBT fibers. Further, the stretched films composed of spherical PBT particles show the ellipsoidal microvoids due to the interfacial debonding, and the void size relates to the particle size of PBT. However, size of PBT droplets does not influence the void content of the stretched films. The void content considerably increases for equibiaxial deformation as compared with planar deformation, particularly at high draw ratio. Additionally, the stretched films containing fibrous dispersion exhibit the nonaffine behavior and the highest void content of 8%, which is probably due to the localized deformation between fibers. © 2014 Wiley Periodicals, Inc. J. Appl. Polym. Sci. **2015**, *132*, 41415.

**KEYWORDS:** composites; fibers; porous materials

Received 31 May 2014; accepted 14 August 2014
**DOI: 10.1002/app.41415**

## INTRODUCTION

Microporous polymeric films have received much interest in a broad range of commercial applications, i.e., breathable agricultural packaging for maintaining the physical characteristics and prolonging the shelf life of perishable produces by altering the gas and water vapor permeability. Several well-known techniques including thermally-induced phase separation[1,2] and selective solvent extraction[3,4] have been developed to produce the microporous films with high porosity; however, a contamination of hazardous solvent and cost of waste solvent treatment are the major disadvantages to be used as food packaging.

Concerning over the environmental issue and manufacturing cost, mechanical stretching of polymer sheets in the solid state is an important method to fabricate microporous films.[5–10] In case of isotactic polypropylene (PP), it has been known that a microporous film is prepared by stretching an extruded sheet containing a large amount of $\beta$ trigonal crystalline form.[11] During the stretching, the crystalline phase transformation from $\beta$- to $\alpha$-form occurs. Up to now, the following mechanisms are believed to be responsible for a large number of microvoids: (1) volume contraction accompanied with the phase transformation, (2) large negative pressure between thick lamellae of $\beta$-form crystals,[12] and (3) numerous void-opening points around nucleating agents.[6,7]

The alternative routes to obtain microporous films include stretching a composite filled with rigid particles[13,14] or immiscible polymer blends.[3,15–17] The biaxially stretched films of polyolefin filled with 15 wt % of $CaCO_3$ particles showed the noninterconnected porous structure, generated from the particle-matrix decohesion owing to poor interfacial specific interaction between polymer and particles.[13] Moreover, Chandavasu et al.[15] and Xanthos et al.[17] prepared microporous films by stretching PP sheets containing spherical polystyrene dispersion at room temperature. They created nanoscale microcracks around the dispersions and subsequently drew it at elevated temperature to enlarge the pore size. Further, biaxial stretching of poly(ethylene terephthlate) with dispersed PP droplets gave void volume of 60%.[16] In contrast, incorporation of an interfacial modifier showed the low levels of void volume because of the increased interfacial strength. Consequently, the void-opening is mainly governed by the stress concentration around

the dispersed phase and the adhesive strength at boundary when the critical stress for craze formation in the matrix and cavitation in dispersed rubber is large enough. Most studies have focused only on preparing membranes from the blends containing spherical particles; however, a dispersion of nanofiber in composites is an interesting candidate owing to the availability of nanofiber nowadays since several methods to prepare nanofiber are proposed.[18–22]

Incorporation of poly(butylene succinate) (PBS) nanofibers in poly(lactic acid) (PLA) matrix prepared by melt-stretching using a capillary rheometer can enhance the modulus, degree of crystallinity and cold-crystallization behavior in comparison with those containing spherical PBS.[23] Ali et al.[24,25] found that polytetrafluoroethylene (PTFE) flexible nanofibers in continuous PP phase drastically improved the drawdown force and primary normal stress difference of the blends. Further, Yamaguchi and coworkers[26,27] found that PLA composites composed of a small amount of fibrous PBT in solid state showed the marked strain-hardening behavior in uniaxial elongational viscosity because of flexibility and interdigitation of the PBT nanofibers. Up to now, however, few authors have specifically addressed the void formation in polymer composites with fibers considering the classical fracture mechanics.[28–30] The initiation of microvoids and their propagation were typically observed around the ends of glass fiber, where the highest shear stress is located, in polyester composites because of weak bonding due to no surface modification of fiber.[30] The formation of microvoids usually occurs along with the stress-whitening, as seen in the glass fiber reinforced polyester composites during tensile tests.[28] It was also mentioned that the stress concentration increases with increasing aspect ratio of the dispersed phase.[31] Nevertheless, the main aim of their works is to clarify the failure mechanism of rigid fiber-reinforced composites. To the best of our knowledge, however, combining the advantages of nanofiber dispersion and applying the fundamental knowledge of fracture mechanism to prepare microporous films have not been well achieved yet.

In this study, the effects of size and shape, i.e., sphere and fiber, of dispersed PBT phase in a PLA matrix on the morphology and rheological properties of the blends are comparatively investigated. Furthermore, PLA/PBT microporous films are prepared by two different biaxial stretching modes, including planar deformation and equibiaxial deformation, and the porous structure and thermal properties of the microporous films are also examined.

## EXPERIMENTAL

### Materials

PLA (NatureWorks LLC, USA; D-content 4.25% and MFR = 6 g/10 min at 210°C/2.16 kg) and PBT (Toray and MFR = 26 g/10 min at 250°C/2.16 kg) were employed in this study. The molecular weight and molecular weight distribution of PLA were analyzed by gel permeable chromatography (GPC) (Tosoh, HPLC-8020). Chloroform was used as eluent at 40°C at a flow rate of 1.0 ml/min and the concentration of sample was 1.0 mg/ml. The system was calibrated using TSK-GEL® GMHXL as a polystyrene standard. The number- and weight average molecular weights for as-received PLA are as follows: $M_n = 1.1 \times 10^5$ and $M_w = 1.5 \times 10^5$. Further, the melting temperatures of PLA and PBT determined from a differential scanning calorimeter are 148 and 221°C, respectively.

**Table I.** Nomenclatures of the PLA/PBT Blends

| Sample | Shape of PBT | Starting blend ratio |
|---|---|---|
| SP-S | Sphere | 90/10 |
| SP-M | Sphere | 75/25 |
| SP-L | Sphere | 60/40 |
| FIBER | Fiber | 60/40 |

### Sample Preparation

Polymer pellets were dried under vacuum at 80°C for 4 h to avoid a hydrolytic degradation with moisture. Then, PLA and PBT were mixed in a molten state at various blend ratios, i.e., 90/10, 75/25 and 60/40 in a volume fraction, using a 60 $cm^3$ internal batch mixer (Toyoseiki, Labo-plastmil) at 240°C, which is higher than the melting points of both polymers. Pentaerythritol tetrakis (3-3,5-di-tert-butyl-4-hydroxyphenyl propionate) (Ciba, Irganox1010) and tris(2,4-di-tert-butylphenyl)phosphate (Ciba, Irgafos168) as thermal stabilizers were also added at 5000 ppm each to hinder the thermal degradation. The blade rotation speed was 40 rpm and the mixing time was 3 min. The total volume of the sample was 42 $cm^3$. The obtained blends were then further mixed with virgin PLA in an internal batch mixer at 180°C, which is lower than the melting point of PBT, for 3 min to achieve the blends containing spherical PBT dispersion with a final volume fraction of 95/5. Because the size of spherical dispersion increases with the volume ratio of the dispersion in the first mixing, the sample prepared from PLA/PBT (90/10) has the smallest PBT dispersion among them.

Furthermore, the fibrous PBT in PLA matrix was prepared by melt-stretching of PLA/PBT (60/40) using a pressure-driven capillary rheometer (Yasuda Seiki Seisakusho, 140-SAS-2002) equipped with a circular die having 40 mm in length, 1.0 mm in diameter, and an entrance angle of 180°. The temperature of cylinder reservoir and die was controlled at 240°C. The sample was extruded at a shear rate of 70 $s^{-1}$ and stretched uniaxially at a draw ratio of 5. The extruded strands were pulled by a set of rotating wheels and quenched immediately by air. Then, the extruded strands were further mixed with virgin PLA in an internal batch mixer for 3 min at 180°C to prepare the blends with 5 vol % of fibrous PBT. Neat PLA and PBT were also processed at the same condition for comparison. The nomenclature used in this study is shown in Table I, in which SP represents spherical dispersion and S, M, and L denote small, medium and large size of dispersions, respectively.

The PLA blends containing spherical PBT and fibrous PBT dispersion were compressed into a flat sheet with a thickness of 200 μm by a laboratory compression-molding machine (Tester Sangyo, SA303IS) at 180°C under 10 MPa for 3 min. Then, the sample was subsequently cooled down at 40°C. The obtained samples were stored in a dessicator prior to further characterization.

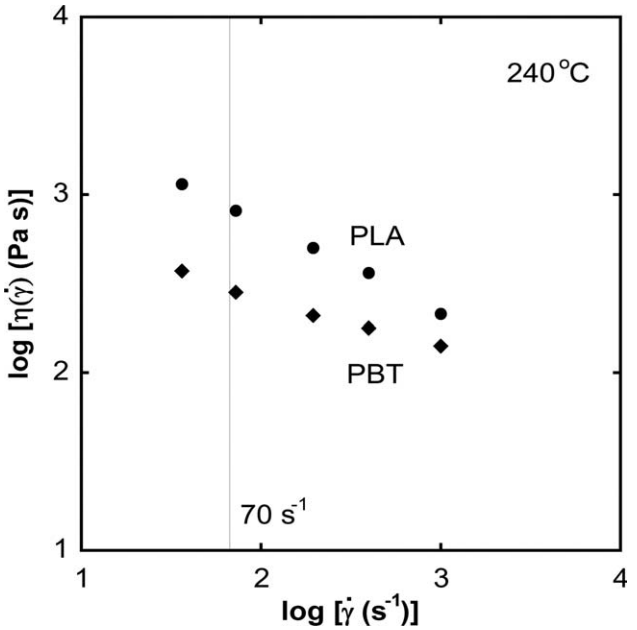


**Figure 1.** Steady-state shear viscosity as a function of shear rate at 240°C for (circles) PLA and (diamonds) PBT.

### Biaxial Stretching

The stretched films were prepared using a biaxial stretching machine (Imoto Machinery, Biaxial film stretcher IMC11A9) as follows. The compressed sheets were cut into squares of 5 × 5 $cm^2$ and then clamped by five chucks on each side with the initial distance of 35 mm. The sheets were equilibrated for 40 min at 80°C, which is about 10°C higher than the glass transition temperature of PLA. The coordinate system of the film is defined as follows: *x*- and *y*-axis is in the in-plane direction and *z*-axis is in the out-of-plane direction (thickness direction). In *planar deformation*, the sheets were stretched uniaxially in *x*-direction while the width was kept constant by stretching in *y*-direction throughout the experiment. In *equibiaxial deformation*, the sheets were simultaneously stretched in *x*- and *y*-directions. The stretching speed was 3 mm/s. Moreover, the amount of force in *x*- and *y*-directions during film stretching was also recorded. Eventually, the stretched films were held at 80°C for 10 min to stabilize the porous structure. The draw ratio ($\lambda$) was defined as the ratio of final length to initial length.

### Measurements

The steady-state shear viscosities as a function of shear rate for pure PLA and PBT at melt-mixing temperature, i.e., 240°C, were collected by a capillary rheometer equipped with a circular die (L/D = 40/1), as shown in Figure 1. It is suggested that both polymers display the shear-thinning behavior and the shear viscosity of PLA is much higher than that of PBT in an entire range of applied shear rate.

The morphologies of compressed and stretched films were observed by a scanning electron microscope (SEM) (Hitachi, S4100) with an acceleration voltage of 20 kV. The samples were coated with Pt/Pd using an ion sputtering machine (Hitachi, E1010) to increase contrast and reduce charging. To observe the dispersed PBT particles, the blends were vigorously stirred in tetrahydrofuran, which is a good solvent for PLA but nonsolvent for PBT, for 1 day. The insoluble fraction was collected and stirred again in fresh THF to ensure that PLA was completely removed. Then, the insoluble PBT fraction was dropped onto a microscope glass slide and dried overnight.

The frequency dependence of oscillatory shear moduli in the molten state, i.e., storage modulus ($G'$) and loss modulus ($G''$), was measured using a cone-and-plate type rheometer (TA Instruments, AR2000ex) in a frequency sweep mode from 100 to 0.1 rad/s at 180°C, under a nitrogen atmosphere to minimize thermal-oxidative degradation. The cone angle was 4°, and the diameter was 25 mm.

A differential scanning calorimeter (DSC) (Mettler, DSC820$^e$) was utilized to collect the thermal properties. Approximately 10 mg in weight of dried samples were encapsulated in standard aluminum pans. The samples were heated from room temperature to 180°C (1st run) and held for 10 min at 180°C in order to erase the remaining thermal history. Then, the samples were cooled down to room temperature and heated to 180°C (2nd run). The heating and cooling rates were 10°C/min. Further, the degree of crystallinity ($X_c$) of PLA is calculated by the following relation:

$$X_c = \frac{\Delta H_m - \Delta H_{cc}}{w \Delta H_m^o} \quad (1)$$

where $\Delta H_m$ and $\Delta H_{cc}$ are the measured enthalpies of melting (as measured from 2nd run) and the cold-crystallization, respectively, while $\Delta H_m^o$ is the enthalpy of melting for a perfect crystalline PLA (93 J/g).[32] The mass fraction of PLA in the blends is denoted as *w*.

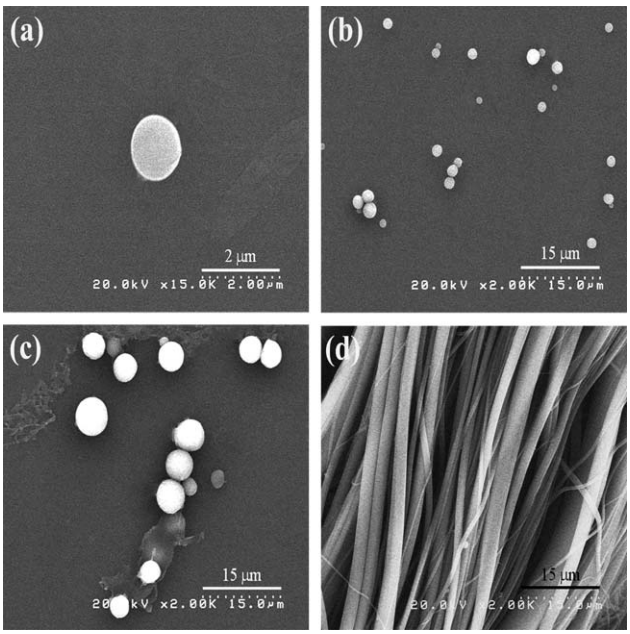


**Figure 2.** SEM micrographs of the extracted PBT domains from the blends prior to melt-stretching for (a) PLA/PBT (90/10), (b) PLA/PBT (75/25), and (c) PLA/PBT (60/40), and (d) the blends after melt-stretching for PLA/PBT (60/40).

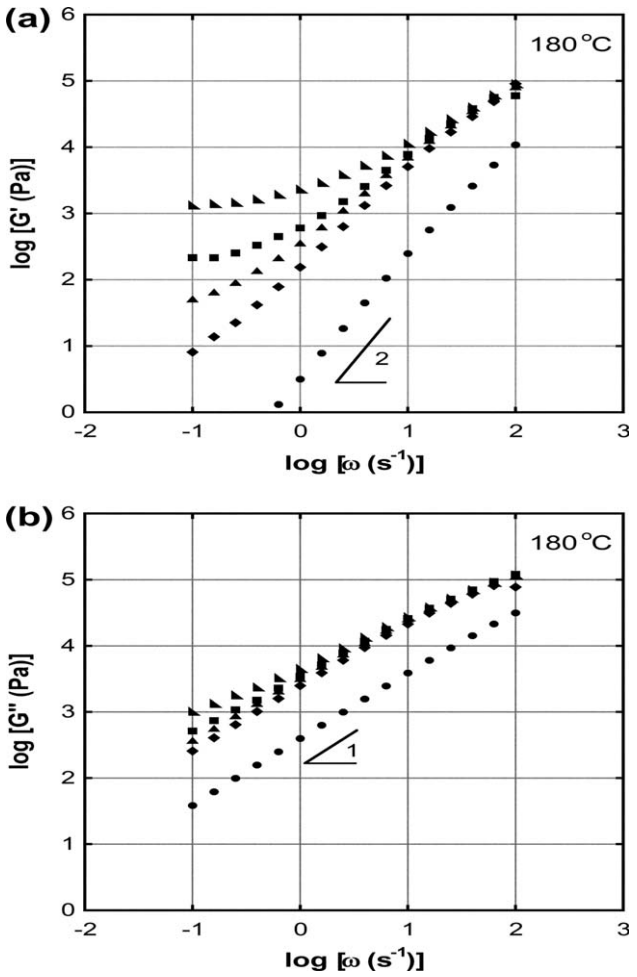


**Figure 3.** Frequency dependence of (a) shear storage modulus $G'$ and (b) loss modulus $G''$ at 180°C for (circles) PLA, (diamonds) SP-S, (triangles) SP-M, (squares) SP-L, and (right triangles) FIBER.

The density of films was measured according to ASTM D792 using a density kit and a top-loading electronic balance. Distilled water was selected as an immersion medium, and its temperature during measurement was recorded. The dry and wet weights of samples were used to determine the bulk density based on Archimedes's principle as follows:

$$\rho = \frac{W_{air}}{W_{air} - W_{water}} \cdot \rho_{water} \quad (2)$$

where $\rho$ and $\rho_{water}$ are the relative densities of the sample and distilled water, respectively. $W_{air}$ is the weight of sample measured in air and $W_{water}$ is the weight of sample measured in distilled water. By comparing the difference in the density of the sample before and after film stretching, the void content can be estimated.

## RESULTS AND DISCUSSION

### Characteristics of Polymer Sheets Prior to Stretching

**Morphology Evolution.** The SEM micrographs of extracted PBT particles from the composites prior to melt-stretching in Figure 2(a–c) show almost perfect spherical PBT droplets, indicating that the PLA/PBT composites have phase separated morphology because of large difference in surface energies between PLA and PBT. By increasing the concentration of PBT as minor phase component, the molten PBT droplets much frequently coalesce and finally become larger, as expected. The number-average diameters and the polydispersity (in parentheses) of PBT spheres increase from 1.30 (1.08) to 2.33 (1.25) and 5.45 (1.42) μm as the volume fraction of PLA/PBT changes from 90/10 to 75/25 and 60/40, respectively.

After capillary extrusion, the molten PBT droplets were deformed into fibrous structure as seen in Figure 2(d). The diameter of most PBT fibers is found to be 1.98 μm on average. Further, it is suggested that the volume of a PBT fiber is larger than that of a spherical PBT because of the coalescence of PBT spheres by the contraction flow near the entrance zone of die and shear flow in the die land.[33,34] Even though the length of most fibers is still unclear because identifying an individual fiber from the bundles is difficult, it is estimated to be longer than several millimeters and its aspect ratio is expected to be larger than 600. On the basis of this approximation, the formation of a fibril results from the coalescence of about 4–5 spherical PBT particles. Moreover, it is worth mentioning that the shape of PBT domains in the PLA composites after kneading

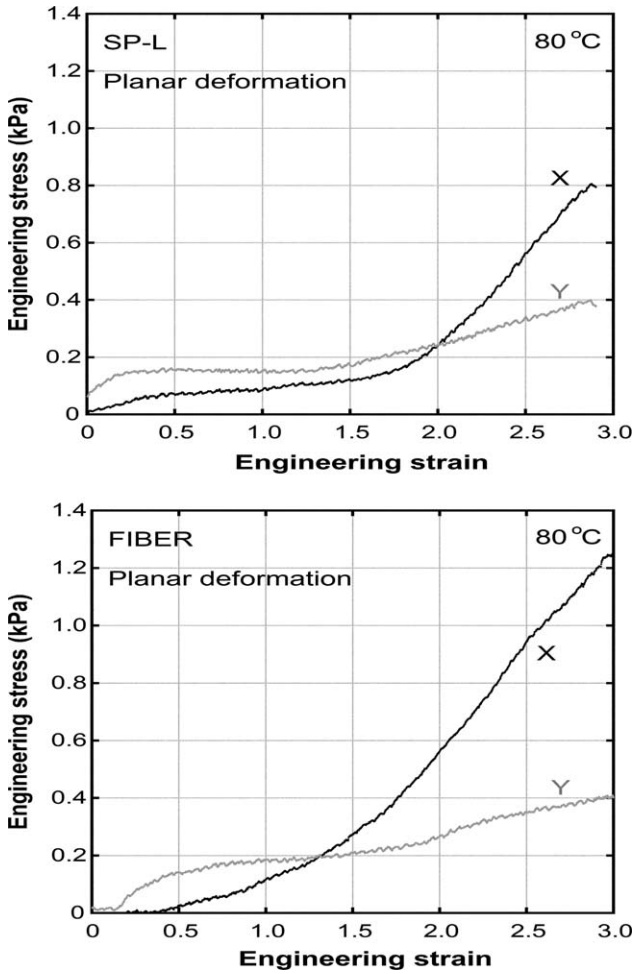


**Figure 4.** Stress–strain curves at 80°C of SP-L and FIBER prepared by planar deformation.

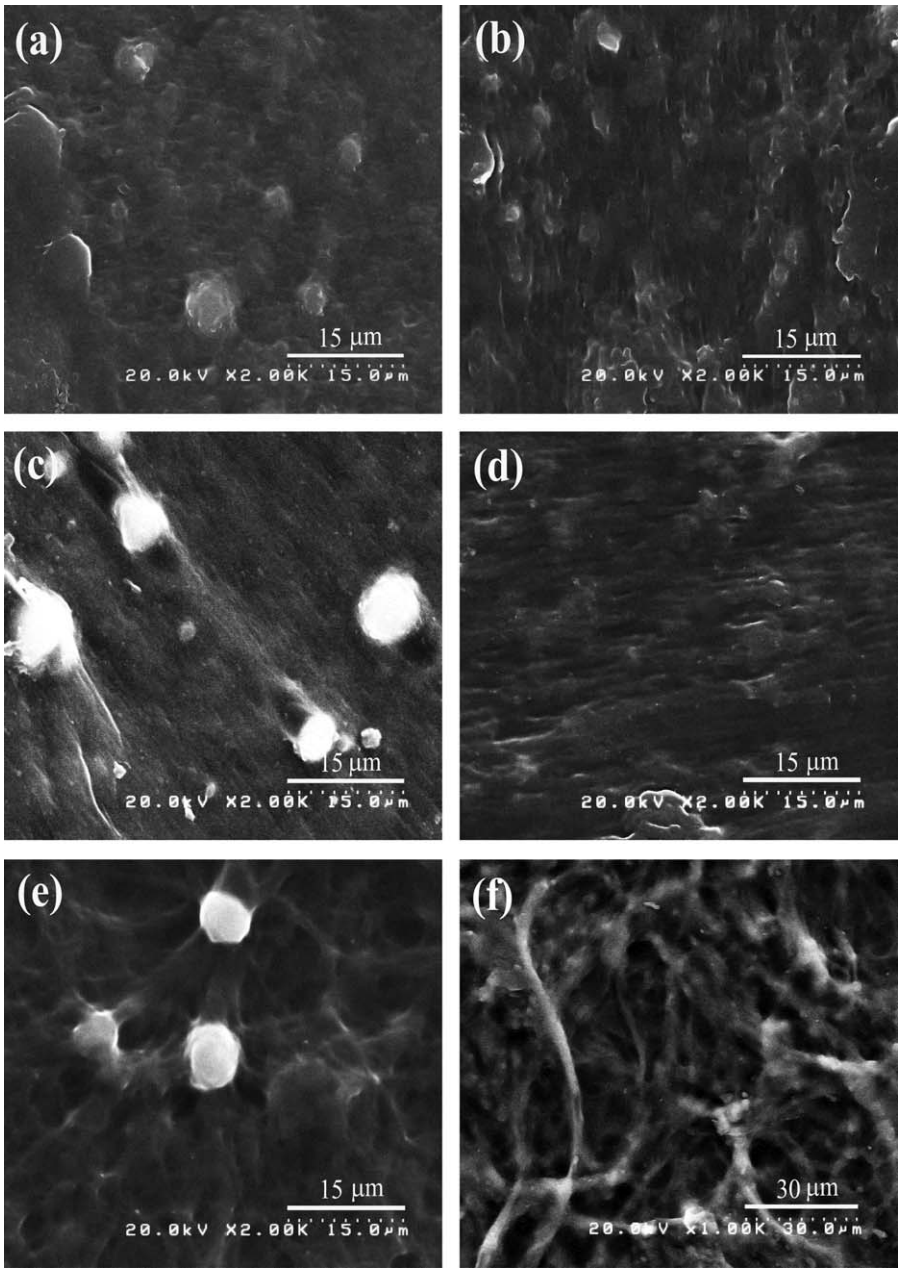


**Figure 5.** SEM micrographs of the surface of the PLA/PBT stretched films at different stretching conditions: (a) SP-L, $\lambda_x \times \lambda_y = 2 \times 1$, (b) FIBER, $\lambda_x \times \lambda_y = 2 \times 1$, (c) SP-L, $\lambda_x \times \lambda_y = 4 \times 1$, (d) FIBER, $\lambda_x \times \lambda_y = 4 \times 1$, (e) SP-L, $\lambda_x \times \lambda_y = 3 \times 3$, (f) FIBER, $\lambda_x \times \lambda_y = 3 \times 3$.

**Table II.** Void Content of the PLA/PBT Stretched Films Containing Various Characteristic Diameters of PBT Dispersed Domain

| Sample | Number-average diameter of PBT (μm) | Void content (%) | Pore shape | Average pore size (μm) |
|---|---|---|---|---|
| SP-S | 1.30 | 1.73 ± 0.07 | Ellipsoid | 0.91 |
| SP-M | 2.33 | 2.11 ± 0.44 | Ellipsoid | 1.46 |
| SP-L | 5.45 | 1.72 ± 0.87 | Ellipsoid | 3.34 |
| FIBER | 1.98 | 4.96 ± 0.54 | Slit | 0.82 (width), 4.63 (length) |

The stretching ratio is $\lambda_x \times \lambda_y = 4 \times 1$.

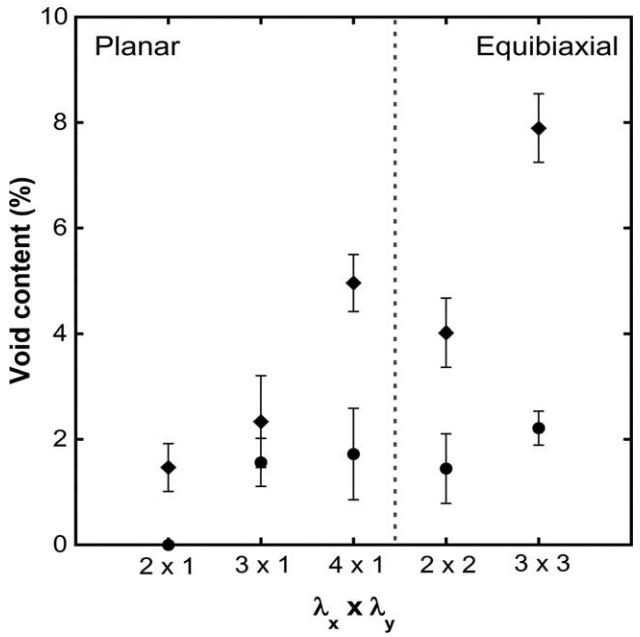


**Figure 6.** Void content as a function of $\lambda_x \times \lambda_y$ from the PLA/PBT stretched films: (circles) SP-L, and (diamonds) FIBER.

with neat PLA at 180°C is still intact as confirmed by SEM observations (results not shown here).

**Linear Viscoelastic Behavior of Neat PLA and the Composites.** The linear viscoelastic responses give the reliable information on the microstructure development in polymer blends. Figure 3 depicts the frequency dependence of oscillatory shear modulus $G'$ and loss modulus $G''$ at 180°C plotted against angular frequency for neat PLA and the composites with dispersed PBT, in which PBT exists in the solid state. The slopes of $G'$ and $G''$ curves for PLA close to 2 and 1 at low frequencies, respectively, indicating that viscous flow is predominant in the terminal zone with the characteristic of a linear viscoelastic fluid.[35] The zero-shear viscosity for PLA is calculated to be $\sim 6.6 \times 10^2$ Pa s at 180°C.

The improvement of the $G'$ for the PLA/PBT composites can be explained by the lubrication effect of the particles prolonging the relaxation time of the particle via the shape recovery phenomenon during an oscillatory shear deformation.[35] Furthermore, a secondary plateau in the $G'$ curve in the low-frequency region is clearly observed as the PBT particle size becomes larger since they require longer relaxation time to relax the interaction between interspacing particles. Specifically, the shape relaxation plateau is more prominent for the composites composed of fibrous PBT, which is attributed to the existence of network structure of random interdigitation of dispersed PBT fibers.

### Characteristics of the Biaxially Stretched Films

**Structure of the Stretched Films.** The film stretching is performed at the temperature beyond the glass transition temperature of PLA (~70°C). It is important to point out that the film stretching cannot be carried out below 80°C since the sheet specimens start to tear off around the chucks at a low strain level. Figure 4 exemplifies the stress–strain curves between sheets containing spherical PBT and fibrous PBT prepared by planar deformation. Because the composites have no voids prior to stretching, the void content can be quantitatively approximated by comparing the apparent density of the specimens before and after film stretching. SEM of the stretched films are shown in Figure 5. Although the voids are not observed at $\lambda_x \times \lambda_y = 2 \times 1$, the voids markedly expands at the polar region of the particles in the stretching direction at $\lambda_x \times \lambda_y = 4 \times 1$. This is because the actual stress concentration in the vicinity of dispersed PBT is intensified because it acts as stress concentrator, and the void opening occurs when the local stress overcomes the interfacial adhesion between PBT domains and PLA matrix.

In planar deformation, it should be noted that there is a relation between the pore size and size of dispersed PBT sphere, as shown in Table II. Using the energy balance between the stored elastic energy and the surface free energy of the spherical particles, the minimum required stress to initiate the cavity around the dispersed particles is *debonding stress* $\sigma_{db}$ shown as follows:[36]

$$\sigma_{db} \propto \left(\frac{EW_a}{D}\right)^{1/2} \quad (3)$$

where $E$ is Young's modulus, $W_a$ is work of interfacial adhesion, and $D$ is diameter of dispersed particle. This relation suggests that the debonding effect is more pronounced for larger particle size since the stress concentration directly relates to the particle size. However, the void contents in Figure 6 are in the same order of magnitude (~2%), implying that the number of void in the SP-S stretched films is probably higher than those in SP-M and SP-L stretched films. On the contrary, the stretched films containing fibrous PBT exhibited a lot of slit-like microvoids on the film surface with a void content of ~5% at $\lambda_x \times \lambda_y = 4 \times 1$. A number-average pore size is ~0.82 μm in width and 3–5 μm in length. Further, the stretched films prepared by equibiaxial deformation ($\lambda_x \times \lambda_y = 2 \times 2$) contain more voids than those prepared by planar deformation ($\lambda_x \times \lambda_y = 4 \times 1$) at the

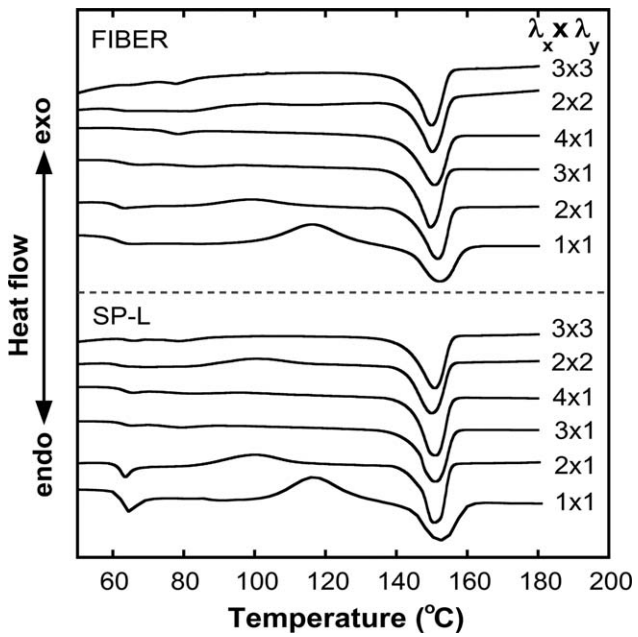


**Figure 7.** DSC curves of the PLA/PBT stretched films.

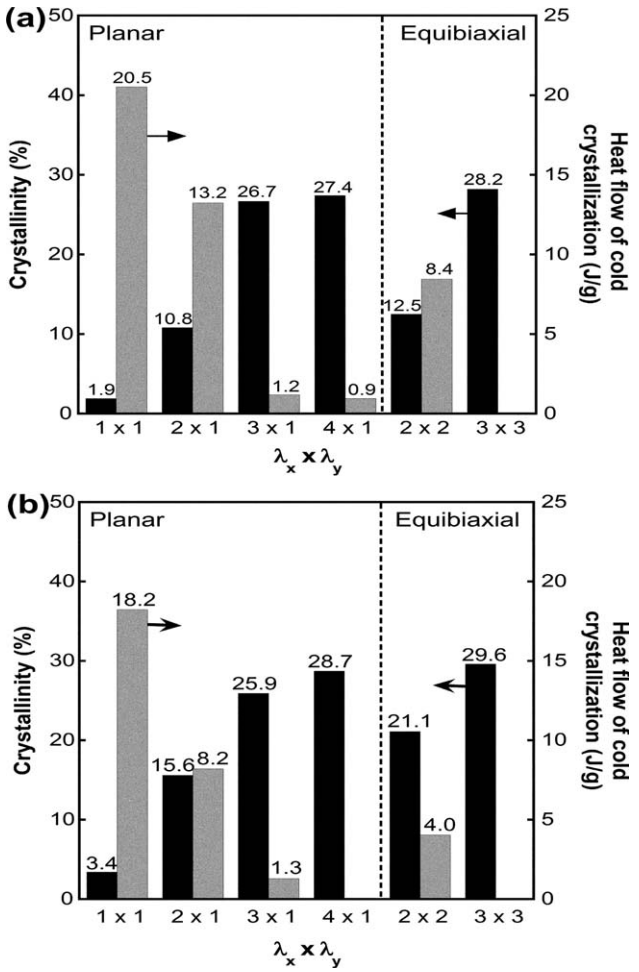


**Figure 8.** Crystallinity and heat flow of cold-crystallization as a function of $\lambda_x \times \lambda_y$ for the PLA/PBT stretched films: (a) SP-L and (b) FIBER.

same stretching level. Moreover, the void content for composites containing fibrous dispersion markedly increases to about 8% at $\lambda_x \times \lambda_y = 3 \times 3$.

In a fibrous system, fibers entangle with neighboring fibers upon mixing resulting in the formation of random network structure, as evidenced by an increase in oscillatory storage moduli in the low-frequency region shown in Figure 3. In the mechanics point of view, the flexible fibers generally store the strain energy in the form of extensional deformation. As can be seen in the stress–strain curves in Figure 4, an increase in a level of stress during film stretching is obviously begun at high draw ratio, indicating that the deformation is restricted and much level of energy is required because the discrete entanglements of fibers, which behave like physically crosslinked points, constrains the mobility of polymer chains to freely move from a specified position. Therefore, this inherently nonaffine behavior is prominent for the composites containing flexible PBT fine fibers in comparison with those with spherical PBT droplets.[37] Additionally, a large number of crosslinked points provide areas with higher stress concentration than the surrounding polymer matrix and it is expected that a localized deformation between these fibers is the origin of the void formation in this study.

**Thermal Behavior Under Stretching.** Figure 7 illustrates the DSC heating curves of the stretched films. During planar and equibiaxial deformations, the shifts of cold-crystallization temperature to lower temperatures and the disappearance of heat of cold-crystallization at high draw ratios suggesting that PLA chains in amorphous phase begin to align in the stretching direction and, eventually, crystallize as a result of a strain-induced crystallization, leading to higher crystallinity. As seen in Figure 8, crystallinity substantially increases for the planar deformation at low deformation levels, i.e., $\lambda_x \times \lambda_y = 2 \times 1$, because of the mobility of molecular chain segments; however, increasing the draw ratio gives a gradual increase in crystallinity since the neighboring crystalline structures acting as a type of physical crosslink restrict the relaxation of polymer chains and segments in the noncrystalline region.[38] Further, the composites with fibrous PBT exhibit slightly lower heat of cold-crystallization and increased crystallinity because fibrous PBT can promote the crystallization process more effectively than spherical PBT.

## CONCLUSIONS

In this work, the effects of size and shape of PBT domain as a minor phase in PLA composites on the morphology and properties of the unstretched blends and the biaxially stretched films have been studied. The SEM micrographs display the phase separated morphology of the immiscible PLA/PBT blends and the formation of PBT fine fibers 1.98 μm in diameter after melt-stretching. Besides, the coalescence of PBT by the contraction flow near the entrance zone of die and shear flow in the die land is responsible for the very long fibers. The network structure of PBT fibers is confirmed by the secondary plateau in the low-frequency region from rheological measurements.

For the stretched films, the void opening is initiated when the local stress around the PBT particles, acting as stress concentrator, overcomes the weak interfacial adhesion between PLA and PBT and, in turn, the pores are elongated as the draw ratio increases. The void content does not influence by the size of spherical PBT; however, numerous microvoids appear in the composites with fibrous dispersion resulting in dramatically high void content. It is expected that the localized deformation between fibers in the random network structure is responsible for high void content in composites with fibrous dispersion. In addition, it is found that the equibiaxial deformation gives the largest void content in comparison with planar deformation, particularly at high draw ratio. Considering that it is more difficult to create many voids in composites with spherical particles because of low stress concentration, we expect that the PLA/PBT microporous films prepared by equibiaxial deformation of the composites with a small amount of fibrous PBT dispersion have the potential to be applied as microporous films.

## ACKNOWLEDGMENTS

The financial support from the Ratchadaphiseksomphot Endowment Fund of Chulalongkorn University (RES5605300086-AM) and the 90th anniversary of Chulalongkorn University fund (Ractchadaphiseksomphot Endowment Fund) are gratefully acknowledged. C. Samthong would like to express his sincere

appreciation to the Royal Golden Jubilee Ph.D. Program (Grant No. PHD/0089/2552) under the Thailand Research Fund (TRF) for financial support throughout the PhD study.

## REFERENCES


1. Yoon, J.; Lesser, A. J.; McCarthy, T. J. *Macromolecules* **2009**, *42*, 8827.
2. Zhang, H.; Zhou, J.; Zhang, X.; Wang, H.; Zhong, W.; Du, Q. *Eur. Polym. J.* **2008**, *44*, 1095.
3. Riscanu, D.; Favis, B. D.; Feng, C.; Matsuura, T. *Polymer* **2004**, *45*, 5597.
4. Sa-nguanruksa, J.; Rujiravanit, R.; Suphol, P.; Tokura, S. *Polym. Test.* **2004**, *23*, 91.
5. Ng, C. S.; Teoh, S. H.; Chung, T. S.; Hutmacher, D. W. *Polymer* **2000**, *41*, 5855.
6. Phulkerd, P.; Hagihara, H.; Nobukawa, S.; Uchiyama, Y.; Yamaguchi, M. *J. Polym. Sci. Part B: Polym. Phys.* **2013**, *51*, 897.
7. Phulkerd, P.; Nobukawa, S.; Uchiyama, Y.; Yamaguchi, M. *Polymer* **2011**, *52*, 4867.
8. Sadeghi, F.; Ajji, A.; Carreau, P. J. *J. Membr. Sci.* **2007**, *292*, 62.
9. Tabatabaei, S. H.; Carreau, P. J.; Ajji, A. *J. Membr. Sci.* **2008**, *325*, 772.
10. Zhu, W.; Zhang, X.; Zhao, C.; Wu, W.; Hou, J.; Xu, M. *Polym. Adv. Technol.* **1996**, *7*, 743.
11. Chu, F.; Yamaoka, T.; Kimura, Y. *Polymer* **1995**, *36*, 2523.
12. Pawlak, A.; Galeski, A. *Macromolecules* **2005**, *38*, 9688.
13. Qaiss, A.; Saidi, H.; Fassi-Fehri, O.; Bousmina, M. *J. Appl. Polym. Sci.* **2012**, *123*, 3425.
14. Zuiderduin, W. C. J.; Westzaan, C.; Huétink, J.; Gaymans, R. J. *Polymer* **2003**, *44*, 261.
15. Chandavasu, C.; Xanthos, M.; Sirkar, K. K.; Gogos, C. G. *Polymer* **2002**, *43*, 781.
16. Lepers, J. C.; Favis, B. D.; Kent, S. L. *Polymer* **2000**, *41*, 1937.
17. Xanthos, M.; Chandavasu, C.; Sirkar, K. K.; Gogos, C. G. *Polym. Eng. Sci.* **2002**, *42*, 810.
18. Boyaud, M. F.; Cassagnau, P.; Michel, A.; Bousmina, M.; Ait-Kadi, A. *Polym. Eng. Sci.* **2001**, *41*, 684.
19. Cassagnau, P.; Michel, A. *Polymer* **2001**, *42*, 3139.
20. Li, J. X.; Wu, J.; Chan, C. M. *Polymer* **2000**, *41*, 6935.
21. Monticciolo, A.; Cassagnau, P.; Michel, A. *Polym. Eng. Sci.* **1998**, *38*, 1882.
22. Takahashi, T.; Takimoto, J.; Koyama, K. *Polym. Compos.* **1999**, *20*, 357.
23. Yokohara, T.; Okamoto, K.; Yamaguchi, M. *J. Appl. Polym. Sci.* **2010**, *117*, 2226.
24. Ali, M. A. B. M.; Nobukawa, S.; Yamaguchi, M. *Pure. Appl. Chem.* **2011**, *83*, 1819.
25. Ali, M. A. B. M.; Okamoto, K.; Yamaguchi, M.; Kasai, T.; Koshirai, A. *J. Polym. Sci. Part B: Polym. Phys.* **2009**, *47*, 2008.
26. Yamaguchi, M.; Fukuda, K.; Yokohara, T.; Amran, M.; Nobukawa, S. *Macromol. Mater. Eng.* **2012**, *297*, 654.
27. Yokohara, T.; Nobukawa, S.; Yamaguchi, M. *J. Rheol.* **2011**, *55*, 1205.
28. Bouaziz, A.; Zaïri, F.; Naït-Abdelaziz, M.; Gloaguen, J. M.; Lefebrve, J. M. *Compos. Sci. Technol.* **2007**, *67*, 3278.
29. Houshyar, S.; Shanks, R. A. *Polym. Int.* **2004**, *53*, 1752.
30. Noda, K.; Takahara, A.; Kajiyama, T. *Polymer* **2001**, *42*, 5803.
31. Menczel, J.; Varga, J. *J. Therm. Anal.* **1983**, *28*, 161.
32. Witzke, D. R.; Narayan, R.; Kolstad, J. J. *Macromolecules* **1997**, *30*, 7075.
33. Tsebrenko, M. V.; Yudin, A. V.; Ablazova, T. I.; Vinogradov, G. V. *Polymer* **1976**, *17*, 831.
34. Gonzalez-Nunez, R.; Chan Man Fong, C. F.; Favis, B. D.; De Kee, D. *J. Appl. Polym. Sci.* **1996**, *62*, 1627.
35. Ferry, J. D. In Viscoelastic Properties of Polymers; Wiley-Interscience: New York, **1980**.
36. Willet, J. L.; Felker, F. C. *Polymer* **2005**, *46*, 3035.
37. Hatami-Marbini, H.; Picu, C. R.; Karpov, E. G.; Grankin, M. V. In Advanced in Soft Matter Mechanics; Li, S., Sun, B., Eds.; Springer: New York, **2012**; Chapter 4, p 123.
38. Lu, X. F.; Hay, J. N. *Polymer* **2001**, *42*, 8055.